Wave-optical evaluation of interference fringes and wavefront phase in a hard-x-ray beam totally reflected by mirror optics

Kazuto Yamauchi, Kazuya Yamamura, Hidekazu Mimura, Yasuhisa Sano, Akira Saito, Katsuyoshi Endo, Alexei Souvorov, Makina Yabashi, Kenji Tamasaku, Tetsuya Ishikawa, and Yuzo Mori

The intensity flatness and wavefront shape in a coherent hard-x-ray beam totally reflected by flat mirrors that have surface bumps modeled by Gaussian functions were investigated by use of a wave-optical simulation code. Simulated results revealed the necessity for peak-to-valley height accuracy of better than 1 nm at a lateral resolution near 0.1 mm to remove high-contrast interference fringes and appreciable wavefront phase errors. Three mirrors that had different surface qualities were tested at the 1 km-long beam line at the SPring-8/Japan Synchrotron Radiation Research Institute. Interference fringes faded when the surface figure was corrected below the subnanometer level to a spatial resolution close to 0.1 mm, as indicated by the simulated results.

OCIS codes: 340.7470, 340.6720, 220.4610, 220.4840, 220.5450.

1. Introduction

One of the important features of third-generation synchrotron x-ray sources is high spatial coherence, which results from a very small source size (for example, $\sigma \sim 10$ μm vertically at the SPring-8/Japan Synchrotron Radiation Research Institute) and a large source-to-object distance (approximately 50–1000 m).[1] In particular, undulators in third-generation facilities emit sharply collimated x rays, sometimes with less than 10 μrad of vertical divergence.[2] Such x-ray beams find many applications in coherent imaging techniques that usually demand a spatially homogeneous beam. However, the high spatial coherence, in turn, has given rise to new problems that were never encountered in the previous generation of sources.[3,4] Various optical components, such as beryllium windows and total-reflection mirrors, become origins of interference fringes when their compositional or structural homogeneity or both are insufficient.

The observation of interference fringes with coherent illumination strongly demands the development of both wave-optical evaluation methods for total-reflection mirrors to determine the criteria of figure and slope errors and mirror manufacturing methods with which to achieve ultrasmooth mirrors within the criteria. Neither the existing scattering theories for nonideal mirrors nor ray tracing based on geometrical optics suffices to explain the interference fringes in the reflected beams.[5–7] However, the recent rapid progress of computational power has enabled us to calculate the Fresnel–Kirchhoff integral[8] numerically when sufficiently accurate surface figure data are available.

In this paper we show a wave-optical simulation method based on the numerical calculation of the Fresnel–Kirchhoff integral for intensity and wavefront phase profiles of x rays totally reflected by flat mirrors. Numerical calculations for single Gaussian bumps that have 1 nm height and various full widths that range from 0.06 to 54 mm on flat mirrors revealed that bump widths of ~1 mm are responsible

K. Yamauchi (yamauchi@prec.eng.osaka-u.ac.jp), H. Mimura, Y. Sano, A. Saito, and Y. Mori are with the Department of Precision Science and Technology, Graduate School of Engineering, Osaka University, Yamada-oka 2-1, Suita, Osaka 565-0871, Japan. K. Yamamura, K. Endo, and Y. Mori are with the Research Center for Ultra-Precision Science and Technology, Graduate School of Engineering, Osaka University, Yamada-oka 2-1, Suita, Osaka 565-0871, Japan. A. Souvorov and M. Yabashi are with SPring-8/Japan Synchrotron Radiation Research Institute, Kouto 1-1-1, Mikazuki, Hyogo 679-5148, Japan. K. Tamasaku and T. Ishikawa are with SPring-8/RIKEN, Kouto 1-1-1, Mikazuki, Hyogo 679-5148, Japan.

Received 19 October 2004; revised manuscript received 13 July 2005; accepted 15 July 2005.

0003-6935/05/326927-06$15.00/0

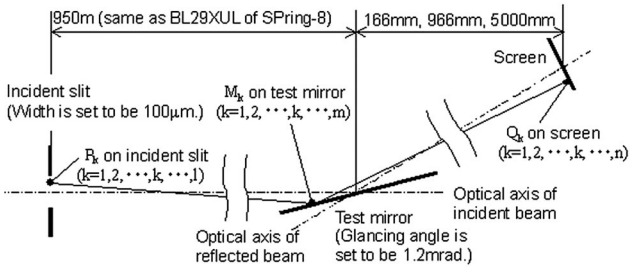

Fig. 1. Schematic of the wave-optical simulator.

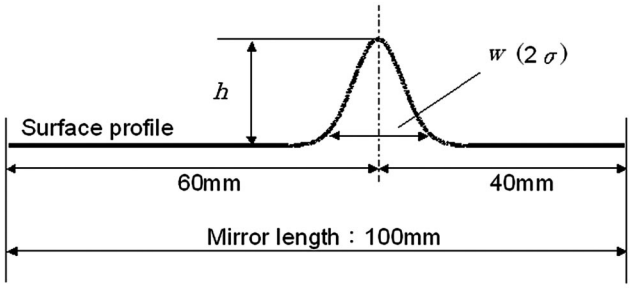

Fig. 2. Surface figure error model with a Gaussian function.

for high-contrast intensity fringes in the reflected beams. The criteria for accuracy of ultraprecise mirrors for coherent x-ray imaging instrumentation in which intensity fluctuations and wavefront phase errors should be reduced, as derived by simulation, are that the peak-to-valley height be accurate to better than 1 nm over a wide spatial frequency range close to 10 mm^{-1}. In addition, we have applied the evaluation method to three types of real flat mirror with different surface qualities. The intensity profiles calculated from the measured figures well reproduced the observed profiles at the 1 km long beam line (BL29XUL) of the SPring-8 facility.[1] The best-quality mirror, manufactured by plasma chemical vaporization machining[9–12] (PCVM) and elastic emission machining[13–17] (EEM), produced the faintest fringe contrast of as little as 1 nm after correction for the peak-to-valley figure error throughout a spatial wavelength range longer than 0.1 mm, as indicated by simulated results.

2. Simulation Models

Geometrical relationships among the x-ray source, the mirror, and the screen in the simulator are set as shown in Fig. 1. The principal dimensions employed are those of the BL29XUL beam line at the SPring-8 facility so the incident vertical slit with 100 μm width is located 950 m upstream of the mirror center. The distance between the center of the mirror and the screen can be chosen as 166, 966, or 5000 mm. The incident x-ray energy and the glancing angle are set to be 20 keV and 1.2 mrad, respectively. In this code, the Fresnel–Kirchhoff integral is calculated on the following theoretical basis and gives the intensity profile of the totally reflected X-ray beam on the screen. The complex disturbance at point M on the mirror at time t that is due to the wave field on the incident slit is given by

$$V(M,\ t) = \int_{\text{Slit}} K_1(P,\ M)V(P,\ t - s(P,\ M)/c)\mathrm{d}P, \quad (1)$$

where c is the velocity of light and $s(P, M)$ and $K_1(P, M)$ are the distance and the transmission function from point P on the incident slit to point M on the mirror, respectively. The complex disturbance at point Q on the screen at time t that is due to the wave field on the mirror's surface is also given by

$$V(Q,\ t) = \int_{\text{Mirror}} K_2(M,\ Q)V(M,\ t - s(M,\ Q)/c)\mathrm{d}M, \quad (2)$$

where Q is a point on the screen and $K_2(M, Q)$ is another transmission function from point M on the mirror to point Q on the screen. In total reflection, at a glancing angle sufficiently smaller than the critical angle, reflectivity at each point on the mirror's surface is approximately constant. In addition, a phase change originating in an evanescent wave field at each point on the mirror's surface is also considered to be constant because the glancing-angle fluctuation is within the order of 0.1 mrad in relatively precise mirror surfaces, in which the heights of the figure error are approximately a few nanometers. Then the complex disturbance at point Q on the screen that is due to the wave field on the incident slit is obtained from

$$V(Q,\ t) = \int_{\text{Mirror}} \int_{\text{Slit}} K(P,\ M,\ Q) \times V(P,\ t - s(M,\ Q)/c - s(P,\ M)/c)\mathrm{d}P\mathrm{d}M, \quad (3)$$

where K is a simply combined transmission function from point Q on the screen to point P on the incident slit through point M on the mirror and fulfills the condition that

$$K(P,\ M,\ Q) = K_1(M,\ Q)K_2(P,\ M). \quad (4)$$

The observable x-ray intensity is obtained by averaging on a time scale expressed by

$$I(Q) = \langle V(Q,\ t)V^*(Q,\ t)\rangle. \quad (5)$$

The transversal coherent length of the x ray at the incident slit of the BL29XUL beam line of the SPring-8 facility is ~50 μm in the vertical direction, which means that nearly fully coherent illumination is expected on the surface of the mirror 950 m downstream of the slit. This fact gives validity to employing fully coherent Fresnel–Kirchhoff integrals.

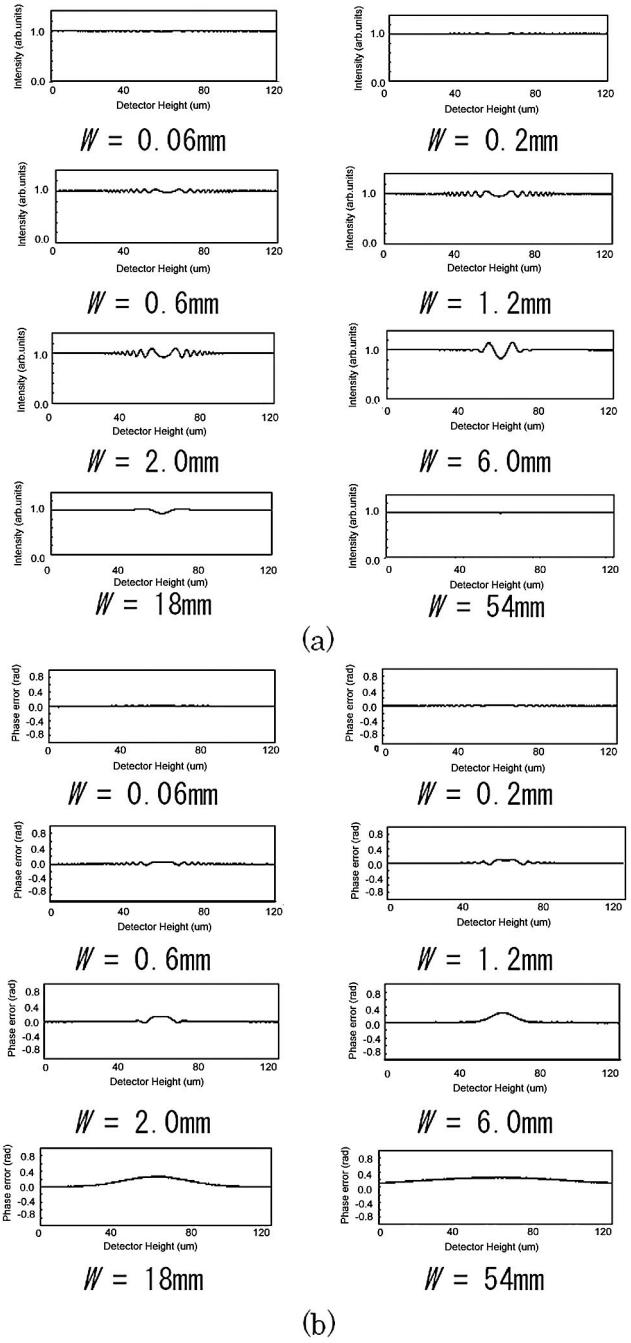

Fig. 3. Calculated intensity and wavefront phase distributions: (a) Calculated intensity distributions (the intensity fluctuation caused by Fresnel diffraction at the mirror edges was removed) and (b) calculated wavefront phase distributions (the phase fluctuation caused by Fresnel diffraction at the mirror edges was removed).

3. Simulation Results

The surface model of the mirror under investigation is shown in Fig. 2. An isolated two-dimensional bump on a flat mirror is employed as a figure error, which is modeled by a Gaussian function that has a height of 1 nm. Several bump widths W, which are related to the spatial wavelength ranges of figure errors, were selected in the range 0.06–54 mm. The intensity and

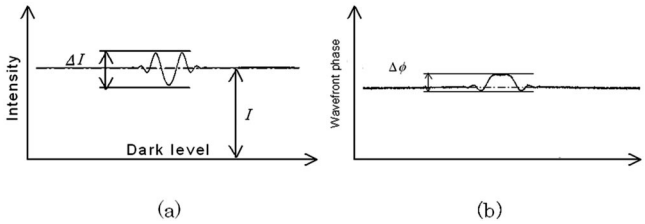

Fig. 4. Definitions of the degrees of intensity modulation and wavefront phase error: (a) normalized amplitude of intensity ($\Delta I/I$), (b) definition of phase error ($\Delta\phi$).

wavefront phase profiles of the reflected beam for the distance between the mirror's center and the screen of 966 mm are shown in Figs. 3(a) and 3(b), respectively. As shown in Fig. 3(a), notable fluctuations, the amplitudes of which are larger than 5% of the average intensity, appear in the intensity profiles for the bump widths in a range of submillimeters to a few tens of millimeters. With a relatively large bump width, the amplitude of the fluctuation decreases because the slope error near the bump becomes smaller. However, in turn, a wavefront error that has a ratio of $4\pi h \sin\theta/\lambda$ to the geometrical configurations, which becomes 0.2 rad under the simulated condition that the height of bump h is 1 nm, glancing angle θ is 0.12 mrad, and x-ray wavelength λ is 0.06 nm, appears as shown in Fig. 3(b). Such wavefront error decreases with smaller bump widths because the light mixes with the components of the beam reflected at the flat area of the mirror surface. However, the error is still not negligible, even when the bump width becomes smaller than 1 mm. In a sufficiently short spatial wavelength range, such as ~0.1 mm, profiles of both the intensity and the wavefront phase become smooth enough even for topographical applications. In this range, the surface undulation can be dealt with as statistical roughness and affects the reflectivity only through the Debye–Waller factor. Using degrees of intensity fluctuation and wavefront phase error defined in Fig. 4 yields results as summarized in Fig. 5. Here we can derive an inconceivable criterion for accuracy of the total-reflection x-ray mirror under coherent illumination: The profile accuracy of the mirror's surface should be higher than 1 nm over a spatial wavelength range longer than submillimeter order. The bump width that causes problematic modulation in the intensity distribution shifts to a smaller range with a shorter distance from the mirror center to the screen. This tendency also appears qualitatively in the amplitude of the wavefront phase error.

4. Reproduction of Measured Intensity

To verify the simulated results experimentally, we prepared three flat mirrors with different surface qualities by the methods of conventional local polishing, PCVM, and EEM. The mirrors were made from silicon, and the surfaces were 111 oriented without coating. In the mirrors, surface figure errors were corrected serially from a spatial frequency range

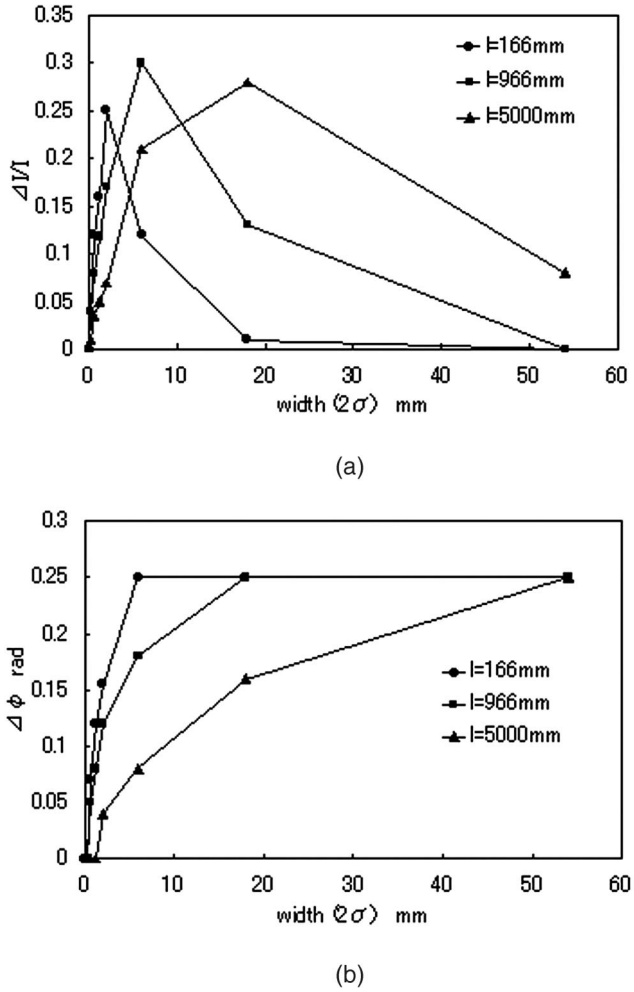

Fig. 5. Relationships of bump width to normalized amplitude of intensity modulation and wavefront phase error: (a) normalized amplitude of intensity modulation, (b) wavefront phase error.

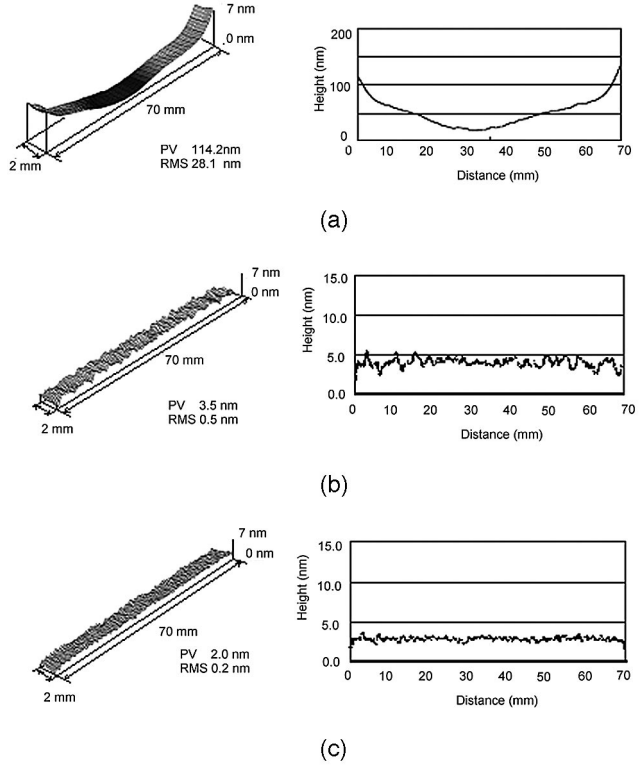

Fig. 6. Measured profiles of the mirror surfaces prepared for the experiment: (a) Conventionally polished mirror surface. (b) PCVM-processed surface. Figure error is corrected in a spatial wavelength range longer than 5 mm. (c) PCVM–EEM-processed surface. Figure error is corrected with a spatial resolution close to 0.1 mm. PV, peak-to-valley

lower than 0.2 mm^{-1} to a high spatial frequency range close to 10 mm^{-1}, as shown in Fig. 6. A conventionally polished surface can be seen to have a concave shape with a depth of ~100 nm. After PCVM processing over a spatial wavelength range longer than 5 mm, the concave shape was removed. However, many pits and bumps of nanometer-level depths and heights with widths of 0.3–5 mm still existed. In contrast, the surface figure error for the mirror additionally processed by EEM was corrected to as small as subnanometer depth or height.

The mirrors were mounted on the goniometer (KOHZU, KTG-15) of the high-precision diffractometer system installed in the experimental hutch of the BL29XUL beam line located 1 km downstream of the center of the light-source undulator. The totally reflected x-ray beam images were observed by use of an x-ray zooming tube–CCD camera (Hamamatsu, C5333) system placed 166 and 966 mm downstream of the center of the mirrors. The dimensional details of the experimental setup are shown in Fig. 7. The photon energy of the incident x ray was tuned to 20 keV, and the glancing angle was set to be 1.2 mrad. The images observed are shown in Fig. 8. A slight curvature of the conventionally polished surface gave rise to beam focusing, which could be identified by the change in size of the reflected beam with the detector's position concurrently with changes in the high-contrast interference fringes. The PCVM correction of the surface profile removed the focusing effect. Nevertheless, the interference fringes still remained in the reflected beam. After additional EEM correction of the surface profile, the fringe contrast in the reflected beam images faded out, except on the edge region where the edge effect, such as the Fresnel diffraction, is dominant. These results are in agreement with the simulated results shown in Figs. 3 and 5. To confirm the consistency quantitatively, we reproduced the reflected beam images from the measured surface profiles, using the same wave-optical

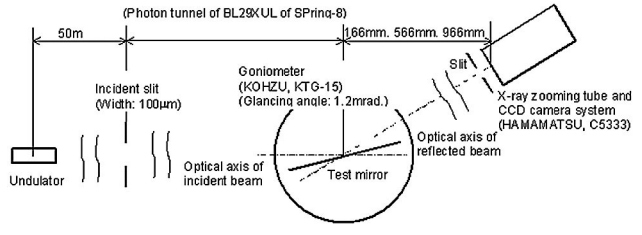

Fig. 7. Dimensional details of the experimental setup.

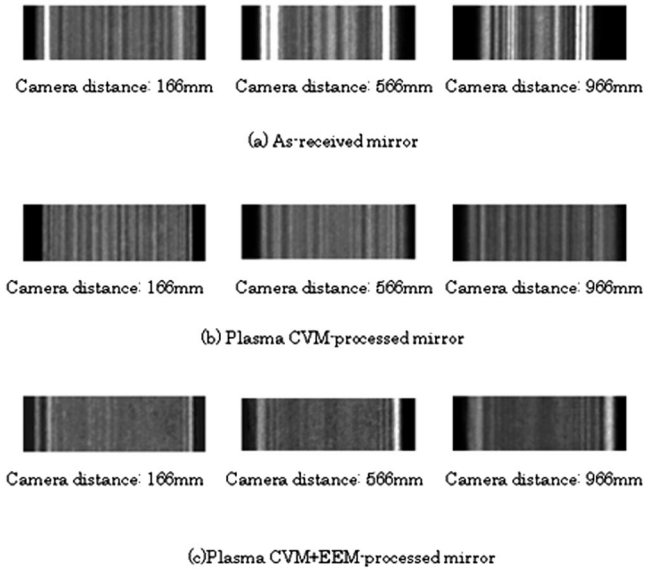

Fig. 8. Reflected beam images observed by use of an x-ray zooming tube and a CCD camera: (a) conventionally polished mirror, (b) PCVM-processed mirror, (c) PCVM–EEM-processed mirror.

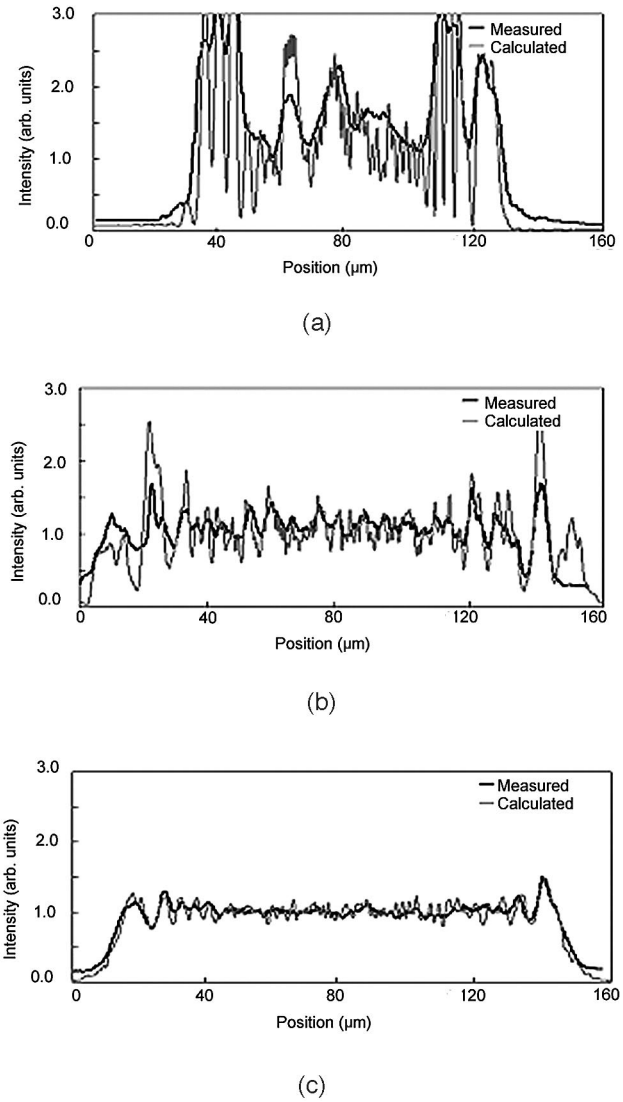

Fig. 9. Calculated and measured intensity profiles of the x-ray beams totally reflected by as-received, PCVM-processed, and PCVM–EEM-processed mirrors with a camera distance of 966 mm: (a) conventionally polished mirror, (b) PCVM processed mirror, (c) PCVM–EEM-processed mirror.

simulator, and compared the results with the experimentally obtained images. In this calculation we also employed two-dimensional surface profiles because the surface profiles of the mirrors in the transversal direction were smooth enough within the spatial range of approximately 300 μm corresponding to the x-ray beam width. This characteristic is due to the path of the small tool in the local polishing method employed for initial fabrication of the test mirrors. To calculate the Fresnel–Kirchhoff integrals, we used a mesh size of 1 μm on the incident silt and on the test mirror. Measured and reproduced intensity profiles are presented in Fig. 9. The agreement is quantitatively acceptable, so the accuracy criteria proposed for obtaining the required quality of the reflected beam under coherent illumination are considered to be reasonable and reflected beam qualities are indicated to be clearly predictable before mirror installation as long as the mirror's surface profile is measured with both a height accuracy higher than 1 nm and a spatial resolution higher than 0.1 mm over the entire surface area. Additionally, a computer-controlled figure-correction method of EEM[17] is certified to make a total-reflection mirror surface that satisfies the accuracy criteria.

5. Discussion

The surface figure in a spatially long wavelength range is conventionally measured over the entire surface of the x-ray mirror before installation to the beam line. Long-trace profilers[18] and large-area optical interferometers[19] are generally employed as measuring devices. In contrast, figure error in the spatial wavelength range up to 1 mm has been treated as roughness and evaluated statistically only at a few points on the mirror's surface. However, the short-wavelength range is important, even when such figure errors exist locally. The intensity fluctuation in the reflected beam, $\Delta I/I$, becomes greater than 20% in such cases, as shown in Fig. 5. Furthermore, high spatial coherence of x rays from third- and coming fourth-generation synchrotron radiation sources can generate higher-contrast fringes in the reflected beam as a result of interference between separately existing bumps or pits, even when the separation distance is longer than 100 mm on the mirror's surface. Therefore, even though the sizes of pits or bumps are smaller than 1 mm, all these anomalies should be precisely measured, and the height or depth should be reduced to within subnanometer order by numerically controlled figure-correction methods. The results of the present simulations strongly suggest that profile measurement with a spatial res-

olution of the order of 0.1 mm should be performed over the entire area of the mirror surface to be used.

6. Conclusions

Wave-optical analysis has revealed that surface bumps with widths of 0.1 to ~50 mm cause high-contrast interference fringes in the reflected beam images at practical distances, such as 1–5 m, between the mirror center and the screen. Three mirrors with different surface qualities were fabricated by local polishing, plasma chemical vaporization machining, and elastic emission machining. Intensity profiles of the beams totally reflected by those mirrors were measured at the BL29XUL beam line at the SPring-8 facility. Nearly fully coherent illumination was achieved on the test mirror, and the profiles were confirmed to be in good agreement with the simulated results. In addition, the images observed and reproduced from the measured surface profile were in good agreement. The results of the present study clearly indicate that vertical peak-to-valley resolution higher than 1 nm and lateral resolution close to 0.1 mm must be satisfied in surface testing and figuring methods for the fabrication of mirrors to steer coherent x rays.

This research was supported by Grant-in-Aid for Scientific Research (S)15106003 and the 21st Century COE Research Program Center for Atomic Fabrication Technology from the Ministry of Education Sports, Culture, Science, and Technology, Japan.

References

1. T. Ishikawa, K. Tamasaku, M. Yabashi, S. Goto, Y. Tanaka, H. Yamazaki, K. Takeshita, H. Kimura, H. Ohashi, T. Matsushita, and T. Ohata, "1 km beamline at SPring-8," in *Advances in X-Rays,* A. K. Freund, T. Ishikawa, A. M. Khounsary, D. C. Mancini, A. G. Michette, and S. Oestreich, eds., Proc. SPIE, **4145,** 1–10 (2001).
2. H. Kitamura, "Present status of SPring-8 insertion devices," J. Synchrotron Radiat. **5,** 184–188 (1998).
3. Y. Mori, K. Yamauchi, K. Yamamura, H. Mimura, A. Saito, H. Kishimoto, Y. Sekito, M. Kanaoka, A. Souvorov, M. Yabashi, K. Tamasaku, and T. Ishikawa, "Development of plasma chemical vaporization machining and elastic emission machining systems for coherent hard x-ray optics," in *X-Ray Mirrors, Crystals, and Multilayers II*, A. K. Freund, A. T. Macrander, T. Ishikawa, and J. L. Woods, eds., Proc. SPIE **4501,** 30–42 (2001).
4. A. Souvorov, M. Yabashi, K. Tamasaku, T. Ishikawa, Y. Mori, K. Yamauchi, and A. Saito, "Deterministic retrieval of surface waviness by means of topography with coherent x-rays," J. Synchrotron Radiat. **9,** 223–228 (2002).
5. E. L. Church and P. Z. Takacs, "Prediction of mirror performance from laboratory measurements," in *X-Ray/EUV Optics for Astronomy and Microscopy*, R. B. Hoover, ed., Proc. SPIE **1160,** 323–336 (1989).
6. E. L. Church and P. Z. Takacs, "Specification of glancing- and normal-incidence x-ray mirrors," Opt. Eng. **34,** 353–360 (1995).
7. J. Susini, "Design parameter for hard x-ray mirrors: the European Synchrotron Radiation Facility case," Opt. Eng. **34,** 361–376 (1995).
8. M. Born and E. Wolf, *Principles of Optics,* 6th ed. (Cambridge U. Press, 1997).
9. Y. Mori, K. Yamamura, and Y. Sano, "Development of plasma chemical vaporization machining," Rev. Sci. Instrum. **71,** 4627–4632 (2000).
10. Y. Mori, K. Yamauchi, K. Yamamura, and Y. Sano, "The study of fabrication of the X-ray mirror by numerically controlled plasma chemical vaporization machining: development of the machine for the x-ray mirror fabrication," Rev. Sci. Instrum. **71,** 4620–4626 (2000).
11. H. Takino, N. Shibata, H. Itoh, T. Kobayashi, H. Tanaka, M. Ebi, K. Yamamura, Y. Sano, and Y. Mori, "Plasma chemical vaporization machining (CVM) for fabrication of optics," Jpn. J. Appl. Phys. **37,** L894–L896 (1998).
12. H. Takino, N. Shibata, H. Itoh, T. Kobayashi, H. Tanaka, M. Ebi, K. Yamamura, Y. Sano, and Y. Mori, "Computer numerically controlled plasma chemical vaporization machining using a pipe electrode for optical fabrication," Appl. Opt. **37,** 5198–5210 (1998).
13. Y. Mori, K. Yamauchi, and K. Endo, "Elastic emission machining," Precis. Eng. **9,** 123–128 (1987).
14. Y. Mori, K. Yamauchi, K. Endo, T. Ide, H. Toyota, K. Nishizawa, and M. Hasegawa, "Observation of elastic emission machined surfaces by scanning tunneling microscopy," J. Vac. Sci. Technol. A **8,** 621–624 (1990).
15. Y. Mori, K. Yamauchi, and K. Endo, "Mechanism of atomic removal in elastic emission machining," Precis. Eng. **10,** 24–28 (1988).
16. K. Yamauchi, K. Hirose, H. Goto, K. Sugiyama, K. Inagaki, K. Yamamura, Y. Sano, and Y. Mori, "First-principle simulation of removal process in EEM (elastic emission machining)," Comput. Mater. Sci. **14,** 232–235 (1999).
17. Y. Mori, K. Yamauchi, K. Sugiyama, K. Inagaki, S. Shimada, J. Uchikoshi, H. Mimura, T. Imai, and K. Kanemura, in *Precision Science and Technology for Perfect Surfaces,* Y. Furukawa, Y. Mori, and T. Kataoka, eds. (Japan Society for Precision Engineering, 1999), pp. 207–212.
18. P. Z. Takacs, S. K. Feng, E. L. Church, S. Qian, and W. Liu, "Long trace profile measurements on cylindrical aspheres," in *Surface Characterization and Testing II,* J. E. Greivenkamp and M. Young, eds., Proc. SPIE **1164,** 203–211 (1989).
19. M. Bray, "Stitching interferometry and absolute surface shape metrology: similarities," in *Optical Manufacturing and Testing IV,* H. P. Stahl, ed., Proc. SPIE **4451,** 375–383 (2001).